

# Optimal Hovering Wing Kinematics of Flapping-Wing Model Using Reinforcement Learning

Hyeon-Ho Yang<sup>1</sup>, Sang-Gil Lee<sup>1</sup>, Yu-Jeong Han<sup>1</sup> & Jae-Hung Han<sup>1</sup>

<sup>1</sup>Korea Advanced Institute of Science and Technology  
Daejeon, 34141, Republic of Korea

## Abstract

The wing kinematics of a flapping-wing air vehicle (FWAV) should be designed considering the unsteady aerodynamics so that the FWAV can achieve high flight efficiency. This study proposes an approach to search for the optimal hovering wing kinematics by using reinforcement learning. The unsteady vortex method based on potential flow is modified to estimate the contribution of leading-edge vortices and is used to simulate the unsteady aerodynamics of the flapping wing model. The environment for reinforcement learning of the flapping wing model is established based on a deep neural network. The transfer learning is introduced to reduce the time cost, and the reward function is designed for learning. The optimal wing kinematics that leads to maximum lift and lift/drag ratio is found. The aerodynamic efficiency of the optimal wing kinematics is validated by applying it to the dynamically scaled-up robotic model.

**Keywords:** Flapping-Wing, Unsteady Aerodynamics, Reinforcement Learning, Neural Network

## 1. Introduction

Biological flyers in nature, such as insects, birds, and bats, utilize flapping-wing motion and active morphing to achieve efficient flight [1, 2]. For example, swift birds morph their wing backward to achieve high maneuverability, and bats use their stretchable membranes to avoid the obstacles in caves. Unlike conventional aircraft, these biological flyers fly at the low Reynolds number range due to their inherent size. And, their flight is specialized in such Reynolds number range by utilizing the unsteady aerodynamic effects of the flapping motion [3].

In order to mimic the flight characteristics of biological flyers, such as acrobatic maneuvers, disguise, and environmental adaptation, there have been a lot of efforts on flapping-wing air vehicles (FWAVs) developments [4-6]. The FWAVs can be classified into avian- or insect-scale ones according to their size and operating range. Typically, the main flight mode of the avian-scale FWAVs is forward flight. Their endurance and payload are relatively longer and larger than those of insect-scale ones. On the other hand, the insect-scale FWAVs have a better performance in hovering flights than avian-scale ones, and they can carry out indoor mission flights similar to those of quadcopters.

Although various FWAVs have been developed, their flight performance and efficiency are still inferior to those of conventional aircrafts. One of the reasons is that the wing kinematics of the FWAVs was designed without proper consideration of the unsteady aerodynamic loads induced by flapping-wing [7, 8]. In order to overcome this issue, this study focuses on the design of optimal wing kinematics with an appropriate aerodynamics model.

There are many numerical methods for estimating the unsteady aerodynamics of a flapping-wing: computational fluid dynamics (CFD), quasi-steady (QS) aerodynamic model, and vortex method. CFD is a high-fidelity method that gives a precise prediction of the aerodynamics of the flapping-wing [9, 10]. However, CFD is unsuitable to solve optimization problems since it requires a very long computation time. On the other hand, the QS aerodynamic model is a low-fidelity method with a low time cost. Although the accuracy of the QS model can be improved by using the aerodynamic coefficients which are experimentally determined [11-14], it has the limitation that the coefficients are

highly dependent on the flapping motion and the flow condition. The vortex methods based on potential flow theory, such as unsteady discrete vortex method (UDVM), unsteady vortex-lattice method (UVLM), and unsteady vortex panel method (UPM), have moderate fidelity and computation cost. Since these vortex methods are fast and reliable methods, they have been used to estimate the unsteady aerodynamics of flapping-wing motions [15-17].

This study introduces an approach to search for the optimal hovering wing kinematics of the flapping-wing model by using neural network-based reinforcement learning. The UVLM is modified to estimate the contribution of leading-edge vortices (LEVs) and is used to simulate the unsteady aerodynamics of the flapping-wing model. The simulation environment for reinforcement learning is established based on a deep neural network and the transfer learning is introduced to reduce the time cost of the learning. The reward function is designed, and the optimal hovering wing kinematics that leads to maximum lift and lift/drag ratio is investigated. The trained wing kinematics is applied to the dynamically scaled-up robotic model, and its aerodynamic characteristics and performance are analyzed.

## 2. Aerodynamic Model of Flapping-Wing

### 2.1 Numerical Method

In order to compute the aerodynamic loads induced by the flapping motion, unsteady vortex lattice method (UVLM) based on the potential flow theory is used. The flow around the flapping-wing is assumed to be incompressible, inviscid, and irrotational. When a velocity potential ( $\Phi$ ) is described in the body-fixed frame which is fixed on the wing, the continuity equation becomes the Laplace equation expressed as:

$$\nabla^2\Phi = 0. \quad (1)$$

Vortex flow elements are used for the solution of Laplace equation, and complicated flows around the moving wing can be represented by superpositioning the vortex elements [18].

Figure 1 shows a schematic of the modified UVLM. A plate wing model whose chord and span lengths are respectively  $c$  and  $b$  is discretized into  $M$  number of chordwise and  $N$  number of spanwise panel elements. Vorticity of uniform strength is replaced with a bound vortex ring of strength  $\Gamma_{ij}$  located at the edge of each element. The collocation point, whose normal vector to each element is  $\mathbf{n}_{ij}$ , is located in the middle of each element where the zero normal flow boundary

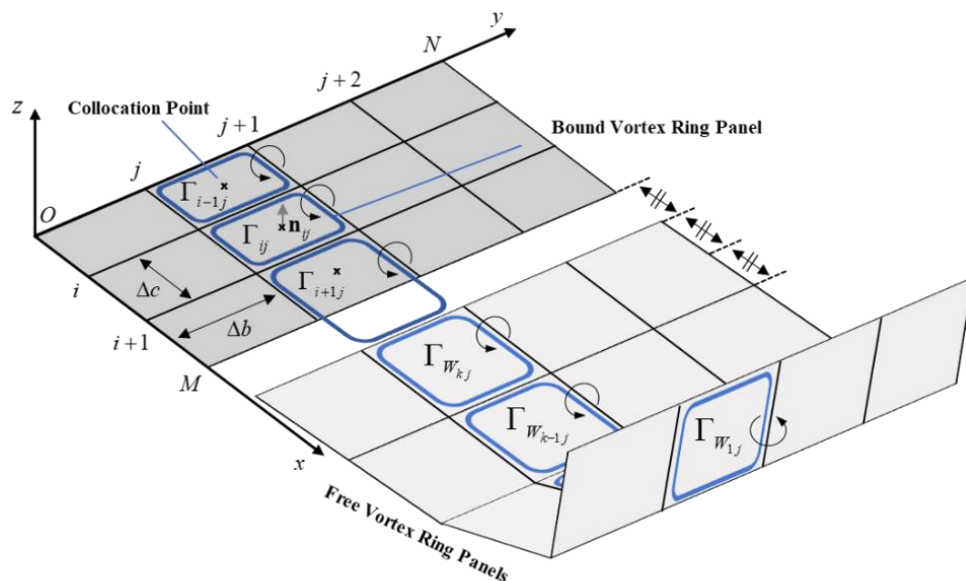


Figure 1 – Schematic diagram of the modified UVLM

condition is enforced. The wakes are modeled as free vortex ring of strength  $\Gamma_{W_{k,j}}$  where  $k$  is an index of the time step, and its shedding starts at one-third of the distance between the trailing-edge and the last free vortex ring. The current shedding location can consider not only the wing motion but also the convection of the previous shed vortices [19].

To consider the time dependency of the unsteady motions, the zero normal flow boundary condition is modified and expressed as:

$$(\nabla\Phi_B + \nabla\Phi_W - [\mathbf{V}_0 + \mathbf{v}_{rel} + \Omega \times \mathbf{r}]) \cdot \mathbf{n} = 0, \quad (2)$$

where  $\mathbf{V}_0$  is the velocity of the origin of the body-fixed frame,  $\mathbf{v}_{rel}$  is the relative motion in the body-fixed frame,  $\Omega$  is the rate of rotation of the body-fixed frame,  $\mathbf{r}$  is the position vector of the body-fixed frame, and  $\mathbf{n}$  is the normal vector to the wing body's surface in the body-fixed frame. The wing is assumed rigid, hence, the normal vector  $\mathbf{n}_{ij}$  takes a value [0, 0, 1] at each collocation point. Also, the additional relative motion is equal to zero. The wing kinematics during each time step is prescribed, and the wing is moved along the kinematics. Each trailing-edge vortex ring sheds a free vortex ring with a strength equal to its circulation in the previous time step. Kelvin's circulation theorem, which gives the conservation of total circulation around a closed fluid link, is inherently fulfilled in the model.

The strength of each vortex ring is obtained by solving a set of algebraic equations derived from the zero normal flow boundary condition expressed in Eq. (2). When  $m$  is equal to  $M \times N$ , the algebraic equations can be expressed as:

$$\begin{bmatrix} a_{11} & a_{12} & \cdots & a_{1,m-1} & a_{1m} \\ a_{21} & a_{22} & \cdots & a_{2,m-1} & a_{2m} \\ \vdots & \vdots & \ddots & \vdots & \vdots \\ a_{m-1,1} & a_{m-1,2} & \cdots & a_{m-1,m-1} & a_{m-1,m} \\ a_{m1} & a_{m2} & \cdots & a_{mm-1} & a_{mm} \end{bmatrix} \begin{pmatrix} \Gamma_1 \\ \Gamma_2 \\ \vdots \\ \Gamma_{m-1} \\ \Gamma_m \end{pmatrix} = \begin{pmatrix} \text{RHS}_1 \\ \text{RHS}_1 \\ \vdots \\ \text{RHS}_{m-1} \\ \text{RHS}_m \end{pmatrix}, \quad (3)$$

where the body influence coefficient ( $a_{\kappa L}$ ) is defined as the normal velocity component at the collocation point  $L$  due to the unit strength  $\Gamma_{\kappa}$ . In this case,  $K$  and  $L$  are indices of the  $(i, j)$ th component in Figure 1. The right-hand side ( $\text{RHS}_{\kappa}$ ) consists of velocity terms and can be expressed as:

$$\text{RHS}_{\kappa} = -(\mathbf{U}(t) + \mathbf{u}_W, \mathbf{V}(t) + \mathbf{v}_W, \mathbf{W}(t) + \mathbf{w}_W)_{\kappa} \cdot \mathbf{n}_{\kappa} \quad (K=1, 2, \dots, m), \quad (4)$$

where  $(\mathbf{U}(t), \mathbf{V}(t), \mathbf{W}(t))_{\kappa}$  represents the kinematic velocity due to the motion of the wing, and  $(\mathbf{u}_W, \mathbf{v}_W, \mathbf{w}_W)_{\kappa}$  represents the induced velocity due to the wake panels.

Vorticity vectors are used to obtain the pressure difference ( $\Delta p_{\kappa}$ ) that is computed using the unsteady Bernoulli equation expressed as:

$$\Delta p_{\kappa}(t) = \rho \left[ \{(\mathbf{U}(t) + \mathbf{u}_W, \mathbf{V}(t) + \mathbf{v}_W, \mathbf{W}(t) + \mathbf{w}_W)_{\kappa} \times \boldsymbol{\gamma}_{\kappa}\} \cdot \mathbf{n}_{\kappa} + \frac{1}{\Delta t} \left( \sum_{K=1}^m \Gamma_K(t) - \sum_{K=1}^m \Gamma_K(t - \Delta t) \right) \right], \quad (5)$$

where  $\boldsymbol{\gamma}_{\kappa}$  is the vorticity vector of the  $K$ th panel element and  $\rho$  is the flow density. The

## Optimal Hovering Wing Kinematics of Flapping-Wing Model Using Reinforcement Learning

aerodynamic forces are obtained by integrating all the pressure differences along the wing's surface. Flapping motion induces a high angle of attack to the wing, and it makes LEV around the wing that is one of the lift augmentation mechanisms [20]. Since the aerodynamic effects induced by the LEV play an important role, they should be considered in the unsteady aerodynamic simulation. If the free vortex rings shed from the leading-edge are included to consider the LEV, the strong interactions among the free and bound vortex rings can make a numerical instability in the simulation [21]. To solve this problem, in this study, the simplified leading-edge suction analogy is introduced [22]. The lift augmentation by the LEV is considered by introducing the leading-edge suction force expressed as:

$$F_s = \frac{\pi}{16} \frac{\eta_s \rho \Gamma_{LE}^2}{\Delta x \cos(\Lambda_{LE})}, \quad (6)$$

where  $\eta_s$  is the suction efficiency,  $\Gamma_{LE}$  is the vortex strength of the leading-edge,  $\Delta x$  is the chordwise panel length, and  $\Lambda_{LE}$  is the local leading-edge sweep angle.

### 2.2 Aerodynamic Simulation and Experimental Validation

Some insects' wing kinematics, such as dronefly and hawkmoth, show a small deviating motion. In this case, the flapping motion can be simplified to be a two-dimensional problem with sweep and pitch motions. For the aerodynamic simulation, a single-articulated flapping-wing model is used. The schematic of the model is shown in Figure 2 where  $\phi$  is the sweep angle,  $\theta$  is the pitch angle,  $R$  is the distance between the center of sweeping motion and wingtip, and  $R_2$  is the radius of gyration to the sweeping motion.

An experiment was conducted to validate the unsteady aerodynamic simulation of the flapping wing model that uses the modified UVLM. A two-degree-of-freedom (2-DOF) dynamically scaled-up

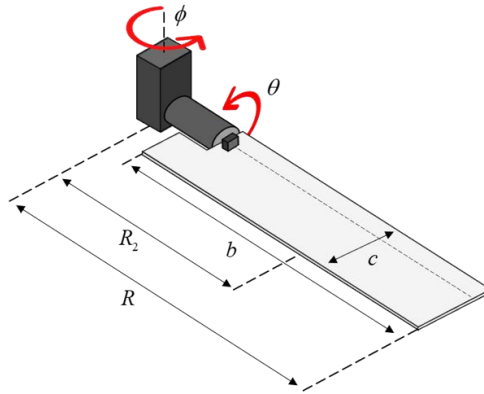


Figure 2 – Flapping-wing model: rigid rectangular plate wing (acryl)

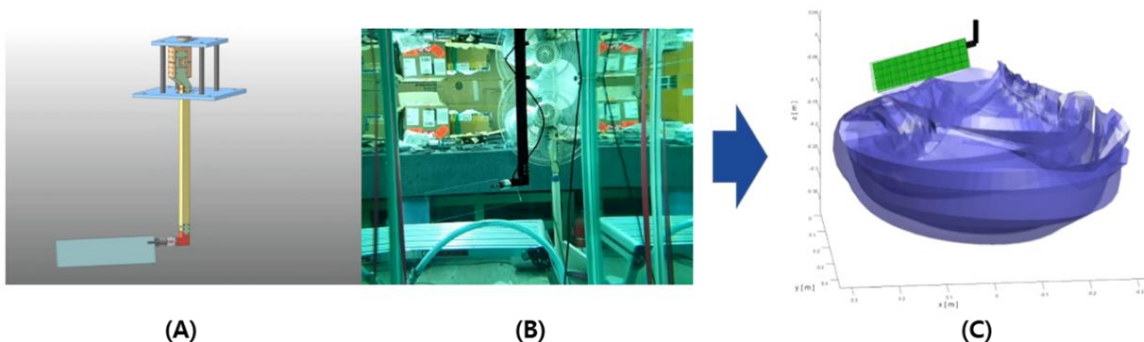


Figure 3 – (A) CAD of the robotic model, (B) scaled-up robotic model in the water tank, (C) wake pattern in the modified UVLM simulation

## Optimal Hovering Wing Kinematics of Flapping-Wing Model Using Reinforcement Learning

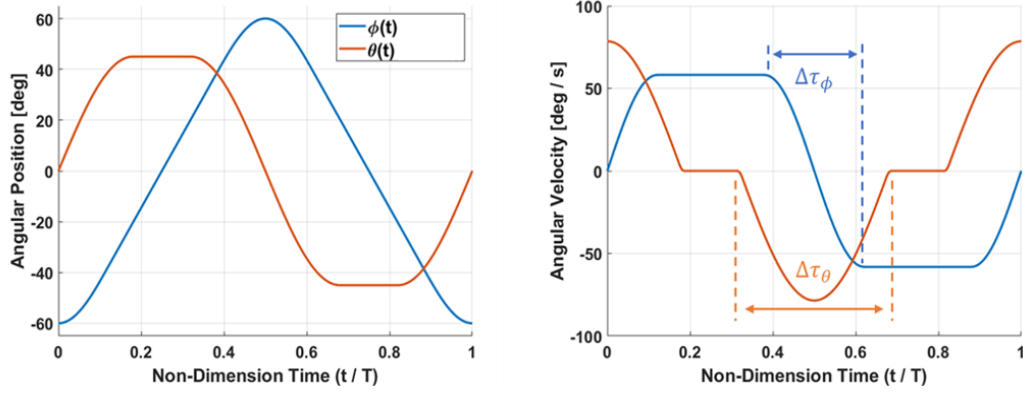


Figure 4 – Sweeping and pitching function profiles of wing kinematics

robotic model was used to generate the continuous flapping motion of the wing. The sweep and pitch motions were independently achieved with two servo motors as shown in Figure 3 (A) and (B).

Insects' hovering wing kinematics can be approximated by using periodic functions that have non-dimensional durations as shown in Figure 4. The piecewise wing kinematics was proposed by Sun and Tang [23] and was adopted in this study. The non-dimensional time ( $\tau$ ) is defined as  $\tau = t / T$ , where  $t$  is the actual time and  $T$  is the total time for one flapping cycle. For a given sweep and pitch amplitude, the shapes of the wing kinematics profile are determined by the non-dimensional sweep duration ( $\Delta\tau_\phi$ ) and the pitch duration ( $\Delta\tau_\theta$ ). For the experimental validation, a total of nine wing kinematics was used by selecting the following non-dimensional sweep and pitch durations:  $\Delta\tau_\phi \times \Delta\tau_\theta = [0.16 \ 0.32 \ 0.50] \times [0.16 \ 0.32 \ 0.50]$ . When the value of the non-dimensional duration is equal to 0.50, the motion becomes sinusoidal.

For the flapping-wing model, the acrylic plate wing with rectangular shape was used. The span length ( $b$ ) is 250mm, the aspect ratio ( $AR$ ) is 4,  $R$  is 275mm and  $R_2$  become 0.605  $R$  for this rectangular wing. The flapping frequency ( $f$ ) of 0.2Hz and sweep amplitude ( $\phi_0$ ) of  $60^\circ$  gave  $Re$  value of about

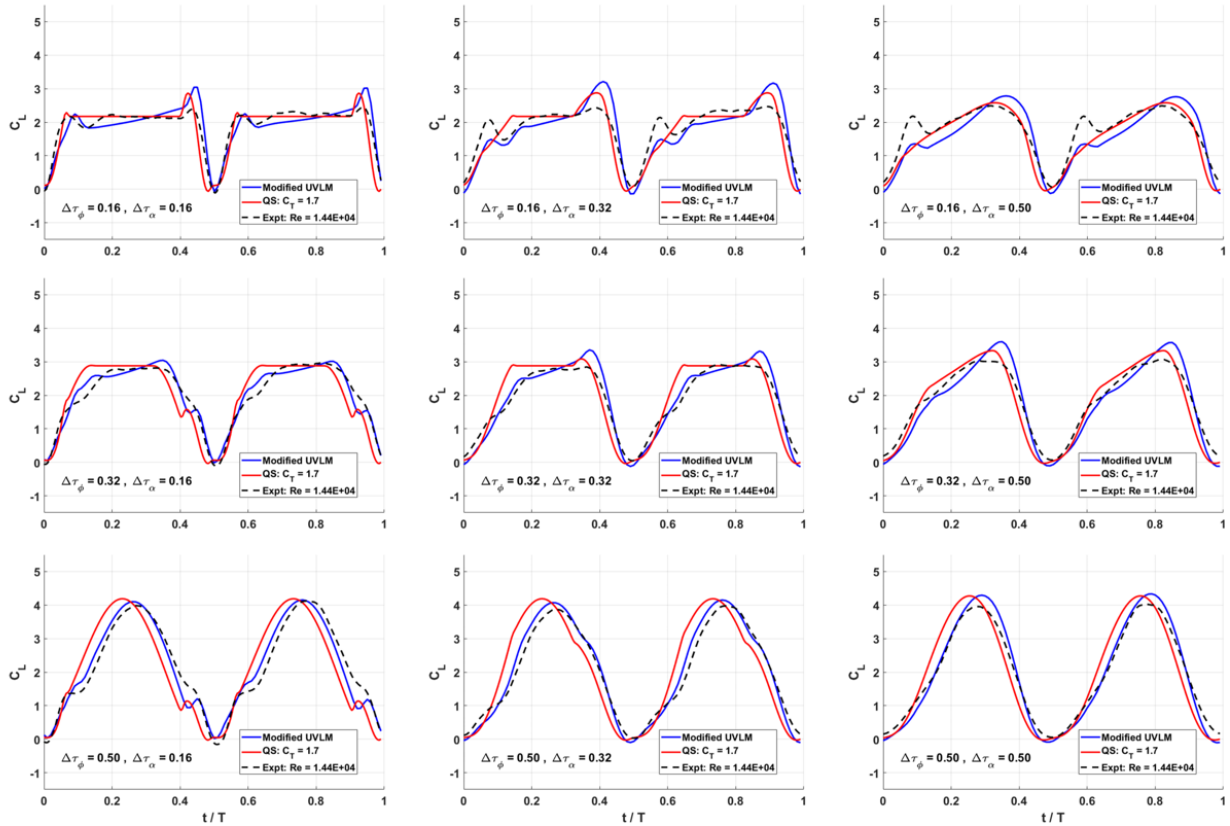


Figure 5 – Lift coefficient comparison (3-5 cycle average value)

$1.4 \times 10^4$  based on Equation (7) where  $\nu$  is the kinematic viscosity of the fluid.

$$\text{Re} = \frac{4f\phi_0 Rc}{\nu} \quad (7)$$

Figure 5 shows the lift coefficient ( $C_L$ ) of the modified UVLM, the quasi-steady (QS) aerodynamic model, and the experimental results. Also, the percent errors of cycle average lift coefficient and lift/drag ratio are shown in Figure 6. Most analysis results based on the modified UVLM have less errors than those of using the QS aerodynamic model. In the case of lift/drag ratio, the percent errors are less than 5% for all wing kinematics; we can conclude that the modified UVLM can give a good estimation for the unsteady aerodynamics of the flapping-wing model.

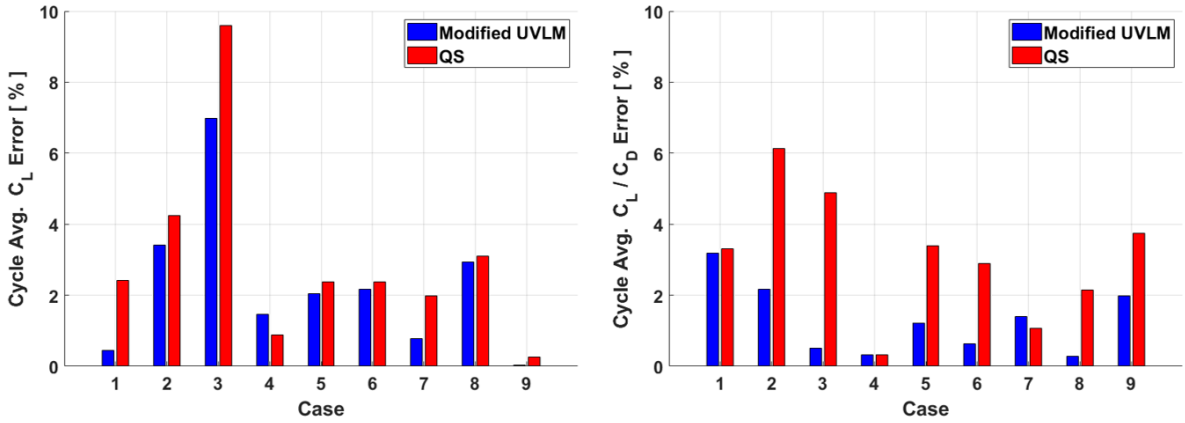


Figure 6 – Percent error of cycle average lift coefficient (left) and lift/drag ratio (right)

### 3. Optimal Hovering Wing Kinematics

#### 3.1 Reinforcement Learning Environment

Reinforcement learning (RL), which is one of the types of machine learning, is used to find the optimal hovering wing kinematics. It is an algorithm that actively responds to the environment by learning the action in a way that the agent maximizes the expected reward in a given state. The RL environment can be defined by constructing the Markov decision process (MDP) whose components are state ( $S$ ), action ( $A$ ), transition probability ( $P$ ), reward ( $R$ ), and discount factor ( $\gamma$ ). The wing kinematics (sweep and pitch motions) for RL is generated using a third-order Fourier series and is expressed as:

$$\phi^*(t) = \sum_{n=1}^3 [a_{\phi n} \cos(n\omega_f t) + b_{\phi n} \sin(n\omega_f t)], \quad (8)$$

$$\theta^*(t) = \sum_{n=1}^3 [a_{\theta n} \cos(n\omega_f t) + b_{\theta n} \sin(n\omega_f t)]. \quad (9)$$

The sweep and pitch motions ( $\phi^*$ ,  $\theta^*$ ) are normalized as expressed in Equations (10) and (11) to always have the same amplitude ( $\phi_0$ ,  $\theta_0$ ) even if the values of the Fourier coefficients are varying during the RL simulation.

$$\phi(t) = \frac{\phi_0}{\max(\phi^*) - \min(\phi^*)} \phi^*(t) \quad (10)$$

$$\theta(t) = \frac{\theta_0}{\max(\theta^*) - \min(\theta^*)} \theta^*(t) \quad (11)$$

The normalized motion profiles are observed by the actor and critic networks and used as states (S). The action (A) is the variation of the coefficients ( $\Delta a_{\phi n}$ ,  $\Delta b_{\phi n}$ ,  $\Delta a_{\theta n}$ ,  $\Delta b_{\theta n}$ ), and the next action is taken according to the neural network-based policy (P). For the reward value, we used the value of the reward function designed for learning and it is expressed as Equations (12) and (13) where N is the number of simulation time steps during the one cycle and M is half of N. The  $r_i$  are the reward function parameters and they are chosen as  $r_1 = 0.1$ ,  $r_2 = 12$ ,  $r_3 = 10$ ,  $r_4 = 2.5$ , and  $r_5 = 2$  in this model.

$$R = \frac{1}{N} \sum_{k=1}^N \left[ r_1 \times C_L(k) + r_2 \times N \left( \frac{C_L(k)}{\text{sign}(\dot{\phi}(k)) C_D(k)} - C_{Ref} \right) \right] - r_3 \times \frac{1}{N} \sum_{k=1}^N C_D(k) - r_4 \times \frac{1}{M} \left| \sum_{k=1}^M [C_L(k) - C_L(k+M)] \right| \quad (12)$$

$$R = -r_5, \text{ if } \max(|\ddot{\phi}|) > \ddot{\phi}_{\max} \text{ or } \max(|\ddot{\theta}|) > \ddot{\theta}_{\max} \quad (13)$$

The reward function gives a higher value when the wing kinematics generates a higher lift and lift/drag ratio. To limit the maximum driving torque for the flapping motion, the simulation boundary condition of the maximum flapping acceleration ( $\ddot{\phi}_{\max}$ ,  $\ddot{\theta}_{\max}$ ) and its penalty are introduced.  $\gamma$  of 0.99 commonly used for RL was used.

Proximal policy optimization (PPO) was used for the RL algorithm [24]. PPO is an algorithm that is easy to implement and has a fast learning speed in the continuous action space. A schematic diagram of the final reinforcement learning environment is shown in Figure 7. When the initial flapping kinematics is determined in the environment, the motion profile is observed and stored as a state. After that, the unsteady aerodynamic simulation using the modified UVLM is performed based on the wing kinematics, and it is checked whether the simulation condition and results deviate from the learning boundary condition. If the learning boundary condition is exceeded, the learning is stopped

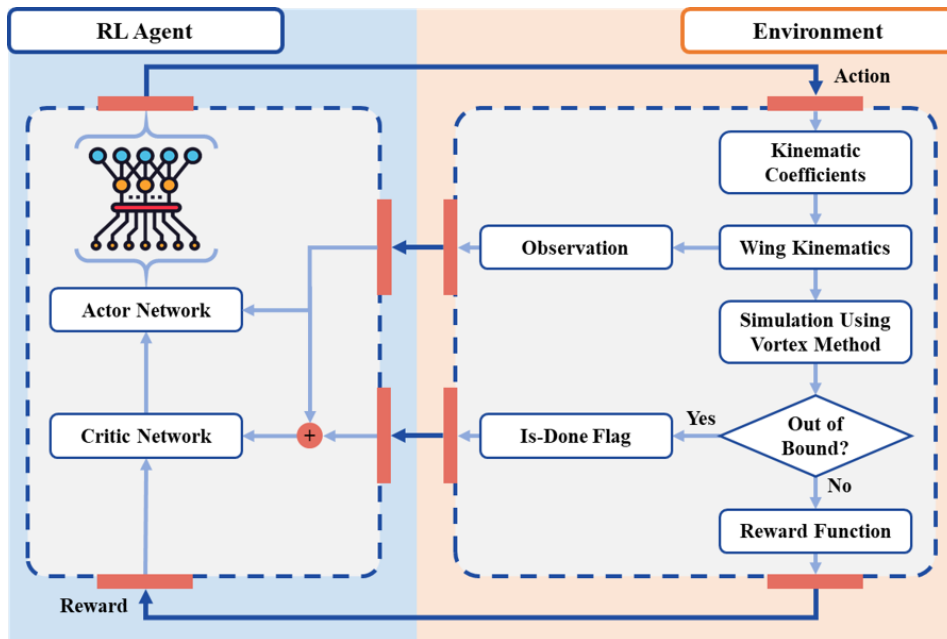


Figure 7 – Schematic diagram of RL environment

and a penalty expressed in Equation (13) is sent to the RL agent. If not, a reward value based on the reward functions expressed in Equation (12) is sent to the RL agent. After receiving the state and reward, the RL agent takes the next action according to the policy based on the actor and critic networks, and this is sent back to the environment.

The flapping motions used in the RL simulation have 100 data points during the one flapping cycle, hence, a total of 200 data are observed as the states. As a result, this RL model learns the relationship between 200 observation states and 12 actions; the 6 actions for sweep motion and the other 6 actions for pitch motion.

The modified UVLM has a relatively short simulation time compared to using CFD. However, it requires a quite long time compared to using the QS aerodynamic model. Therefore, in order to reduce the total time cost, the transfer learning using the modified UVLM model was performed after initial learning using the QS aerodynamic model.

### 3.2 Results

Figure 8 shows the comparison between the initial sinusoidal wing kinematics and trained one. The RL was performed for a total of 1000 episodes, and there are two kinds of trained wing kinematics: Case A and Case B. Case A used the QS aerodynamic model for the whole episodes. In Case B, the initial 500 episodes were trained with the QS aerodynamic model and the subsequent 500 episodes were trained with the modified UVLM model. As shown in the trained results, for both cases, the time duration for constant angles of sweep and pitch motion becomes longer than those in the

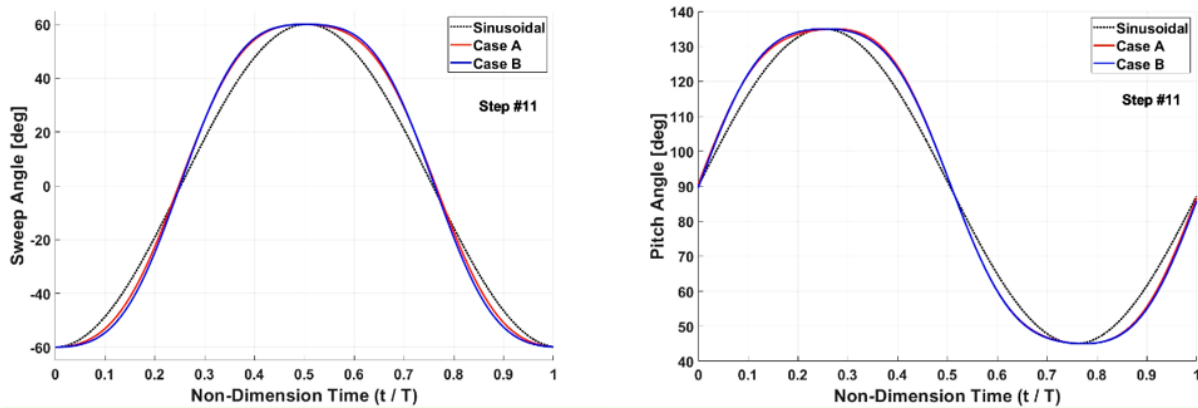


Figure 8 – Trained wing kinematics; Case A: trained with only QS; Case B: trained with QS + UVLM sinusoidal wing kinematics.

Although the wing kinematics profile of Case A and B are similar, they have differences in cycle average lift and lift/drag ratio. As shown in Table 1, Case A shows a 25.8% higher lift and 24.3% higher lift/drag ratio than the sinusoidal wing kinematics. On the other hand, Case B shows a 35.6% higher lift and 27.0% higher lift/drag ratio than the sinusoidal wing kinematics. It means that the wing kinematics with a higher lift and lift/drag ratio can be searched when the transfer learning using the modified UVLM model is performed rather than learning with only the QS aerodynamic model.

### 4. Conclusion

In this study, the approach to search for the optimal hovering wing kinematics by using reinforcement learning is proposed. The UVLM was modified to effectively consider the effects of LEVs induced by

Table 1 Comparison of lift coefficient and lift/drag ratio (experimental results)

Case	Sinusoidal	Case A: QS + QS	Case B: QS + UVLM
$C_L$	1.94	2.44 (+25.8%)	2.63 (+35.6%)
$C_L/C_D$	0.74	0.92 (+24.3%)	0.94 (+27.0%)

the flapping motion. The modified UVLM was validated through the comparison with water tank experimental results using the dynamically scaled-up robotic model, and it was found that the modified UVLM can give a good estimation for the unsteady aerodynamics of the flapping-wing model. The RL agent and environment of the flapping-wing model were established by constructing the proper MDP. The transfer learning is introduced to reduce the time cost, and the reward function is designed for learning. The optimal hovering wing kinematics that generates maximum lift and lift/drag ratio was found. The developed aerodynamic model and the RL environment can be extended to the various FWAVs considering the practical component such as body effect and wing flexibility.

### 5. Acknowledgements

This research was supported by Unmanned Vehicles Core Technology Research and Development Program through the National Research Foundation of Korea (NRF) and Unmanned Vehicle Advanced Research Center (UVARC) funded by the Ministry of Science and ICT, the Republic of Korea (2020M3C1C1A01083415).

### 6. Contact Author Email Address

Hyeon-Ho Yang: hhy9557@kaist.ac.kr

Sang-Gil Lee: sanggil.lee@kaist.ac.kr

Yu-Jeong Han: yujeong\_han@kaist.ac.kr

Jae-Hung Han: jaehunghan@kaist.ac.kr

### 7. Copyright Statement

The authors confirm that they, and/or their company or organization, hold copyright on all of the original material included in this paper. The authors also confirm that they have obtained permission, from the copyright holder of any third party material included in this paper, to publish it as part of their paper. The authors confirm that they give permission, or have obtained permission from the copyright holder of this paper, for the publication and distribution of this paper as part of the ICAS proceedings or as individual off-prints from the proceedings.

### References

- [1] Shyy W, Aono H, Kang C-K and Liu H. *An introduction to flapping wing aerodynamics*. Cambridge University Press, 2013.
- [2] Lentink D, Müller UK, Stamhuis EJ, De Kat R, Van Gestel W, Veldhuis LLM, Henningsson P, Hedenström A, Videler JJ and Van Leeuwen JL. How swifts control their glide performance with morphing wings. *Nature*, Vol. 446, No. 7139, pp 1082-1085, 2007.
- [3] Shyy W, Lian Y, Tang J, Viieru D and Liu H. *Aerodynamics of low reynolds number flyers*. Cambridge University Press, 2007.
- [4] Gerdes JW, Gupta SK and Wilkerson SA. A review of bird-inspired flapping wing miniature air vehicle designs. *Journal of Mechanisms and Robotics*, Vol. 4, No. 2, 021003, 2012.
- [5] Ward TA, Rezadad M, Fearday CJ and Vijapuri R. A review of biomimetic air vehicle research: 1984-2014. *International Journal of Micro Air Vehicles*, Vol. 7, No. 3, pp 375-394, 2015.
- [6] Han J, Hui Z, Tian F and Chen G. Review on bio-inspired flight systems and bionic aerodynamics. *Chinese Journal of Aeronautics*, Vol. 34, No. 7, pp 170-186, 2020.
- [7] Nguyen Q-V, Chan WL and Debiase M. Hybrid design and performance tests of a hovering insect-inspired flapping-wing micro aerial vehicle. *Journal of Bionic Engineering*, Vol. 13, No. 2, pp 235-248, 2016.
- [8] Ryu SW, Lee JG and Kim HJ. Design, fabrication, and analysis of flapping and folding wing mechanism for a robotic bird. *Journal of Bionic Engineering*, Vol. 17, No. 2, pp 229-240, 2020.
- [9] Lankford J, Mayo D and Chpra I. Computational investigation of insect-based flapping wings for micro air vehicle applications. *International Journal of Micro Air Vehicles*, Vol. 8, No. 2, pp 64-78, 2016.
- [10] Nakata T, Liu H, Tanaka Y, Nishihashi N, Wang X and Sato A. Aerodynamics of a bio-inspired flexible

## Optimal Hovering Wing Kinematics of Flapping-Wing Model Using Reinforcement Learning

- flapping-wing micro air vehicle. *Bioinspiration & Biomimetics*, Vol 6, No. 4, p 045002, 2011.
- [11] Sane SP and Dickinson MH. The aerodynamic effects of wing rotation and a revised quasi-steady model of flapping flight. *Journal of Experimental Biology*. Vol. 205, No. 8, pp 1087-1096, 2002.
- [12] Han J-S, Kim J-K, Chang JW and Han J-H. An improved quasi-steady aerodynamic model for insect wings that considers movement of the center of pressure. *Bioinspiration & Biomimetics*, Vol. 10, No. 4, p 046014, 2015.
- [13] Han J-S, Chang JW and Han J-H. The advance ratio effect on the lift augmentations of an insect-like flapping wing in forward flight. *Journal of Fluid Mechanics*, Vol. 808, pp 485-510, 2016.
- [14] Addo-Akoto R, Han J-S and Han J-H. Influence of aspect ratio on wing-wake interaction for flapping wing in hover. *Experiments in Fluids*, Vol. 60, No. 164, 2019.
- [15] Ghomm M, Collier N, Niemi AH and Calo VM. On the shape optimization of flapping wings and their performance analysis. *Aerospace Science and Technology*, Vol. 32, No. 1, pp 274-292, 2014.
- [16] Nguyen AT, Han J-S and Han J-H. Effect of body aerodynamics on the dynamic flight stability of the hawkmoth *Manduca sexta*. *Bioinspiration & Biomimetics*, Vol. 12, No. 1, p 016007, 2016.
- [17] Nguyen AT and Han J-H. Wing flexibility effects on the flight performance of an insect-like flapping-wing micro-air vehicle. *Aerospace Science and Technology*, Vol. 79, pp 468-481, 2018.
- [18] Katz J and Plotkin A. *Low-speed aerodynamics*. 2nd edition, Cambridge University Press, 2001.
- [19] Ramesh K, Gopalarathnam A, Granlund K, Ol MV and Edwards JR. Discrete-vortex method with novel shedding criterion for unsteady aerofoil flows with intermittent leading-edge vortex shedding. *Journal of Fluid Mechanics*, Vol. 751, pp 500-538, 2014.
- [20] Shyy W and Liu H. Flapping wings and aerodynamic lift: the role of leading-edge vortices. *AIAA Journal*, Vol. 45, No. 12, pp 2817-2819, 2007.
- [21] Roccia BA, Preidikman S, Massa JC and Mook DT. Modified unsteady vortex-lattice method to study flapping wings in hover flight. *AIAA Journal*, Vol. 51, No. 11, pp 2628-2642, 2013.
- [22] Nguyen AT, Kim J-K, Han JS and Han J-H. Extended unsteady vortex-lattice method for insect flapping wings. *Journal of Aircraft*, Vol. 53, No. 6, pp 1709-1718, 2016.
- [23] Sun M and Tang J. Unsteady aerodynamic force generation by a model fruit fly wing in flapping motion. *Journal of Experimental Biology*, Vol. 205, No. 1, pp 55-70, 2002.
- [24] Schulman J, Wolski F, Dhariwal P, Radford A and Klimov O. Proximal policy optimization algorithms. *arXiv preprint arXiv:1707.06347*, 2017.